Available online at www.sciencedirect.com
ScienceDirect
Nuclear Instruments and Methods in Physics Research A 569 (2006) 162–166
NUCLEAR INSTRUMENTS & METHODS IN PHYSICS RESEARCH Section A
www.elsevier.com/locate/nima

Programmable electronics for low-cost small animal PET/SPECT imaging

Pedro Guerra*, Jose L. Rubio, Georgios Kontaxakis, Juan E. Ortuño, Maria J. Ledesma, Andres Santos

Universidad Politécnica de Madrid, ETSI de Telecomunicación, Madrid 28040, Spain

Available online 8 September 2006

Abstract

This work describes and characterizes the detector module of a novel positron/single photon emission (PET/SPECT) scanner for small animals. This detector consists of a YAP/LSO phoswich, a photomultiplier and acquisition front-end, and will be used as building block of a low-cost hybrid tomograph. The front-end processes data sampled at a fixed frequency, where a state-of-the-art programmable device estimates scintillation pulse parameters by means of digital algorithms. Finally, the estimated properties of the proposed detector module are used to model a rotating four-head scanner. The performance of the proposed PET/SPECT scanner is estimated and first results are promising in both modalities, deserving further research and optimization.

PACS: 87.62.+n; 07.05.Hd; 87.58.Ce; 87.58.Fg; 24.10.Lx

Keywords: Single photon/positron emission tomography; Phoswich detectors; FPGA based front-end electronics; Data acquisition system

1. Introduction

Since the discovery of the X-rays in 1895, non-invasive imaging has been a significant break through in the practice of medicine. After the development of the first computer-assisted tomograph, different imaging modalities have been adopted by the medical community. Among these, emission techniques have shown the capability to monitor fundamental cellular events and chemical pathways in living subjects, based on the emitted radiation of a radiolabeled pharmaceutical [1]. In particular, both PET and SPECT are powerful tools for the research with animal models of human diseases, which enable not only assessing the disease progression but investigating the animal response to therapy as well. However, imaging small rodents is challenging due to the high resolution and high sensitivity that are required for visualizing complex functions taking place in the small tissue structures of the animal [1,2]. These are requirements that has motivated many laboratories worldwide to design their own system tailored to the application [3–13].

It is known that PET provides higher sensitivity and spatial resolution than SPECT, due to the electronic collimation. However PET has the drawback of being more expensive, due to the need of equipment for radiopharmaceutical production [14]. Moreover, there is a growing interest in tracing related processes simultaneously, which is something that can be easily done with SPECT but not with PET. As a result, both techniques are not mutually exclusive and it has even been shown that in some situations simultaneous acquisitions may have advantages over separate acquisitions [15]. These facts have motivated several authors to design hybrid systems [14,16–18].

In this work the detector phoswich and acquisition electronics of a novel PET/SPECT scanner for small animals are described and characterized, considering a YAP/LSO combination. This module will be used as building block of a low-cost flexible hybrid scanner The aim of this work is to specify a proper setup for the

*Corresponding author. Tel.: +34 91 5495700 4242; fax: +34 91 3367323.
E-mail address: pguerra@die.upm.es (P. Guerra).

0168-9002/$ - see front matter © 2006 Elsevier B.V. All rights reserved.
doi:10.1016/j.nima.2006.08.042

detector phoswich and implement a digital acquisition front-end useful for both modalities. As a hybrid system will only be practical if its performance is comparable with existing state-of-the art devices for each modality. Preliminary performance estimations have also been carried out via Monte Carlo simulations for a particular scanner configuration.

This document is structured as follows, Section 1 presents the tools used during this work and provides an overview of the proposed scanner, Section 2 describes the architecture of the acquisition front-end and the Section 3 analyzes the estimated performance of the individual detector and the overall system. Finally this document closes with the main conclusions and on going work.

2. Material and methods

2.1. Software tools

The Geant4 Application for Tomographic Emission (GATE v1.0.2) [19] has been used for the performance estimation of the proposed system. This application encapsulates the Geant4 libraries to achieve a modular and versatile simulation toolkit adapted to the field of nuclear medicine, enabling an accurate description and performance estimation of the scanner. As this description includes parameters which depend on the actual detector, we have run independent simulations in order to estimate them. The simulated output have been reconstructed with the Open Source software package for tomographic imaging (STIR v1.4) [20].

DETECT2000 [21] was selected for the characterization of the scintillation phoswich. This Monte-Carlo simulation software generates light photons, whose individual evolution and final fate is recorded along with the flight time and path length. Based on these simulations we can estimate the overall quantum efficiency for each layer of the detector phoswich.

The digital front-end has been implemented on a FPGA, designed with the software package ISE v6.2 (Xilinx Inc., San José, CA, USA) and simulated with Modelsim v5.7 (Mentor Graphics, Wilsonville, OR, USA). The pulse-processing block has been optimized and verified through cosimulation with Modelsim and Simulink 5.0 (The Mathworks, Natick, MA, USA). Simulink has been used to provide realistic stimuli to the VHDL simulator through the modeling of the front-end (crystal layers, PS-PMT, analog electronics and ADCs) [22]. Based on these simulations, we have estimated energy and time resolutions as well as the pulse discrimination capability of the implemented electronics for the given configuration.

2.2. Design concept

Our design goal is to specify a low-cost system capable of performing both PET and SPECT studies and adaptable to different geometries. The proposed scanner consists of a rotating gantry that mounts a variable number of detectors, each of which integrates all the detection and processing electronics. The detectors modules will include detachable parallel-hole collimators in order to enable different acquisition configurations, i.e. PET-only, SPECT-only and combined PET/SPECT.

In the design of the detector, the selected scintillation material plays a significant role. Currently, there is no scintillation material that is simultaneously best suited for both modalities, therefore either a trade-off is found [14] or a phoswich is defined [16–18]. The prototype simulated in this study assumed a detector consisting of two 25×25 crystal layers, YAP and LSO, with a fixed front section of $2 \times 2\,mm^2$/crystal. The yttrium aluminum perovskite (YAP:Ce) has been proposed as a potentially good detector for animal PET: it is among the fastest inorganic crystals and its expected time resolution is comparable to LSO; however, its excellent spectroscopy properties are somewhat limited by a low photofraction of 4% [23]. On the other hand, the intrinsic radioactivity originating from ^{176}Lu, whose background count rate (5–20 cps/crystal) is on the order of a typical SPECT study, raises some concerns in using lutetium oxyorthosilicate (LSO), or any other Lutetium-based scintillator, in the design of a SPECT tomograph [16]. As a result, the low-density YAP will be in the front layer of the phoswich, while the LSO events will be only accepted in PET. This arrangement is needed in order to do SPECT, but in the case of PET it might incur some degradation, when compared to the inverse crystal setup, that needs to be analyzed.

3. Readout electronics and processing

The front-module, as shown in Fig. 1, consists of a scintillation phoswich, a position sensitive photomultiplier (PS-PMT), a resistive readout, a set of ADCs, running at a fixed frequency, and a FPGA that processes and encapsulates the detected events. Pulse detection is done in the digital domain, with all processing algorithms implemented in a single FPGA. The detected pulses are sent to an external host through a fast Ethernet connection for off-line coincidence detection in the case of PET, image reconstruction and data storage.

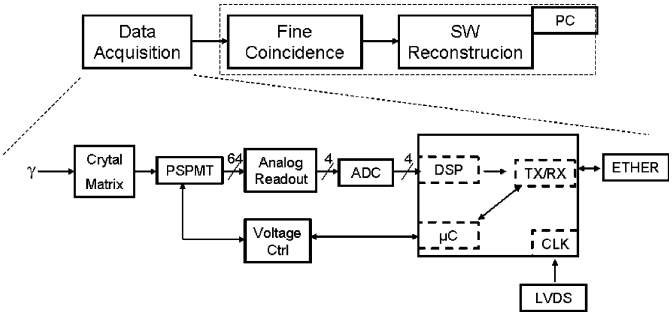

Fig. 1. High Level architecture of the proposed system, with a detailed view of one of the acquisition modules.

As it has been previously described [24], the implemented FPGA integrates a microprocessor (uC), which runs an embedded real-time operating system (RT/OS) and provides the services for TCP/IP communications. The motivation to create an embedded system is to combine the flexibility of the software with efficiency of the hardware. We believe that an efficient and flexible readout system will improve the overall performance of both modalities: a fast data collection system will increase the count rate, improving image quality, and early digitization of the scintillation pulses will provide the needed flexibility to accommodate the processing best suited for each modality.

Each module may be configured either in single or coincidence mode. In the former mode every detected event is acquired, while in the latter mode a wide time window is applied in order to reject those events that have no chance of being coincident. In order to increase the electronics flexibility, the uC can actuate over the analog readout to adjust preamplifiers gain. The preamplified signal is digitalized with no further shaping at a fixed sampling frequency of 65 MHz. The sampled signal undergoes the processing shown in the diagram of Fig. 2:

- Base line (BLR) and signal polarity correction.
- Event detection, based on the instantaneous energy and acquisition triggering.
- Timestamp computation, based on the optical optimum filter as described in Ref. [25].
- Energy estimation and delayed energy estimation, for off-line depth of interaction correction (DOI).

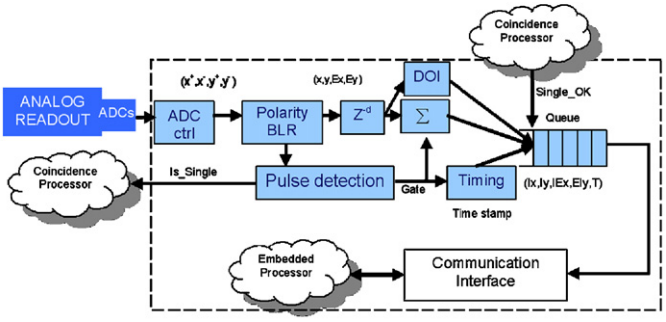

Fig. 2. Detailed block diagram of the DSP block. The pulse detection state machine triggers the acquisition of a pulse. The results are stored in a queue and sent to the external computer with the aid of an embedded processor.

4. Results

4.1. Phoswich characterization

The DETECT2000 simulation code was used to model a 25×25 YAP/LSO phoswich block, where all crystals are $15 \times 2 \times 2\,\mathrm{mm}^3$ and whose main properties are summarized in Table 1 [23,26,27]. With this approach we intend to overcome the lack of optical photons tracking in GATE.

The crystal's light collection efficiency depends on its shape, aspect ratio, surface finish and coupling between adjacent crystals. For these reasons, we simulated different aspect ratios, apart from the desired $15 \times 2 \times 2\,\mathrm{mm}^3$, and we also tested different surface reflecting coefficients to model crystal finish and coupling, as described in Ref. [28].

For each crystal, γ-ray interactions were simulated at different depth within the crystals. Specifically, 10 K photons were generated with 0.1 mm steps starting at 1 mm from the detector's surface. For each of these depths, the process was repeated 30 times in order to improve accuracy. Finally, the average transfer efficiency for each layer is computed by weighting the results with the γ-ray interaction probability at each depth. Fig. 3 shows the simulated transfer efficiency for crystal widths going from 1 up to 3 mm, with different lateral surface finishes as suggested in Ref. [27]. The top face of the upper layer (YAP) was covered with Teflon, while the bottom face and crystal-to-crystal interface are polished and glued by a thin

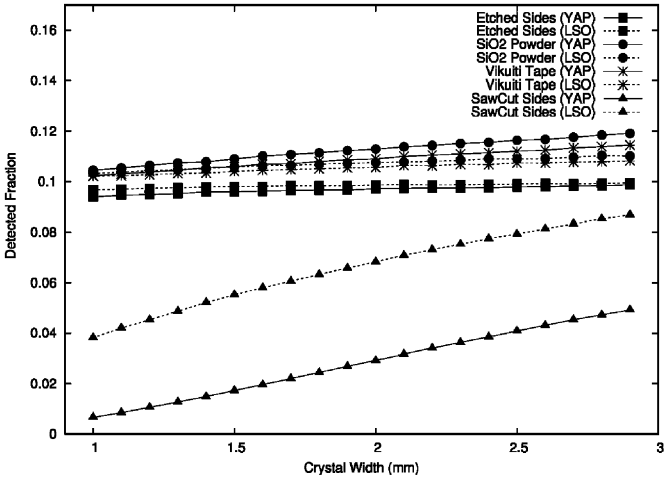

Fig. 3. Simulated quantum efficiency of the each layer of the YAP-LSO phoswich, when considering different crystal finishes. These simulations consider the PS-PMT [29] efficiency at the peak emission wavelength of each crystal and the effect of the interfaces when polished and glued with optical grease.

Table 1
Main properties of the selected scintillators

	Yield (pho/keV)	Decay time (ns)	Rise time (ns)	FE fraction	Wavelength (nm)	Refractive index	$\Delta E/E$ at 511 keV (%)
YAP	18	26.7/140	0.38	4%	370	1.95	6.4
LSO	25	44.7	0.338	34%	420	1.82	6.62

layer of optical grease ($n = 1.55$). Results show that, apart from the saw cut finish, the variation in the transfer efficiency is small in the considered range. The best results are obtained with the Si02 powder and the Vikuiti film, but the first one is considered to be more suited for the size of the crystals.

4.2. Acquisition electronics characterization

In order to run system simulations, the implemented electronics have to be characterized in terms of dead time, timing resolution, crystal layer discrimination and energy resolution. The implemented solution has a minimum dead time of 13 clock cycles, i.e. 260 ns for the working clock frequency; however, actual dead time depends on the selected integration time.

Timing resolution depends on the crystal properties, pulse shaping and time stamping algorithm. Through simulation, we have estimated the resolution of the implemented timing algorithm for LSO and YAP signals, for a shaped pulse ($\tau_s = 10$ ns) sampled at 65 MHz. In total 20,000 events per layer are simulated and the error between the generated timestamp and the real one is computed. The results, summarized in Table 2, confirm the ability to identify coincidences within a 5–10 ns coincidence window.

Using the cosimulation platform, we have simulated 10k events for each layer and analyzed the HW output for the total energy and the energy in a delayed window. Fig. 4 shows the relationship between both energies for LSO and YAP. From these simulation results, we conclude that both layers can be separated with an error lower than 5%. This parameter will be considered to account for the impact on resolution of classification errors.

4.3. Scanner performance

The proposed scanner has been described with GATE, four detector heads with an angular step of 90° between them and 9 cm of rotation radius. Each detector consists of a $50 \times 50\,mm^2$ phoswich block with two layers of $15 \times 2 \times 2\,mm^3$ crystals: YAP on the top and LSO on the bottom. A 20 mm lead collimator was placed on top of two opposite detectors, while the other pair was left uncovered. The collimator is a parallel-hole one with 0.6 mm hole diameter and a 0.15 mm gap between the hexagonally arranged holes.

Table 2
Estimated coincidence timing resolution for the possible detection pairs

Estimation	LSO–LSO	LSO–YAP	YAP–YAP	Average
Coincidence resolution (FWHM in ns)	2.14	1.90	1.63	1.89
A priori probability (%)	25	50	25	

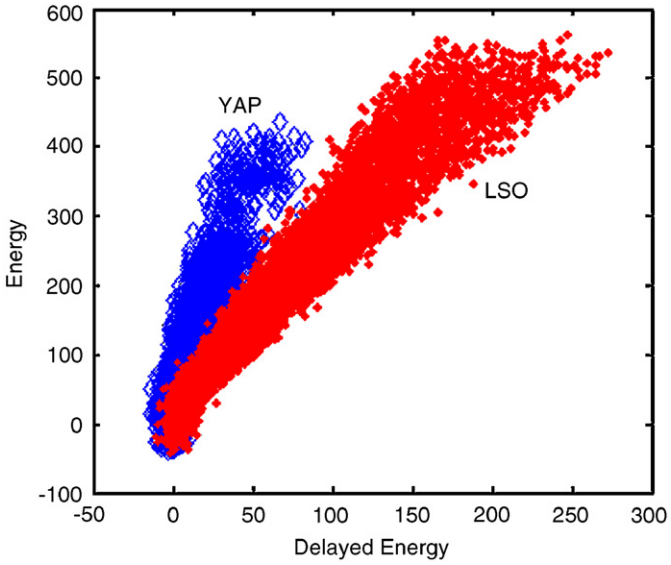

Fig. 4. Relationship between the energy in the main window and the energy in the delayed window for LSO and YAP. Crystal identification error is lower that 5%. For the selection of a proper delayed window, the timing properties of the selected crystals have to be considered.

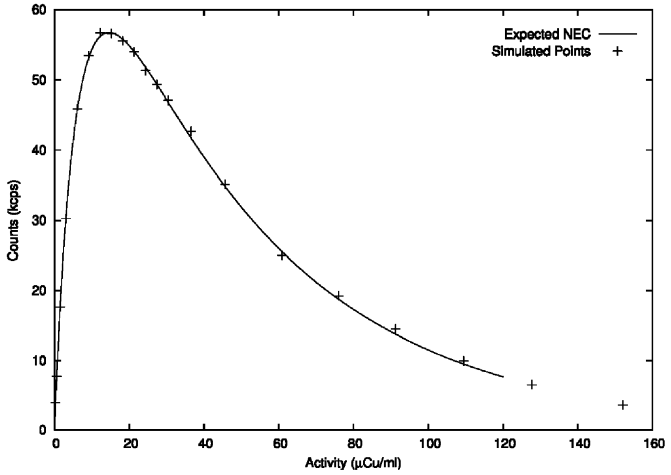

Fig. 5. Estimated NEC curve. The simulated profile is consistent with the expected values based on the analytical expressions defined in Ref. [30].

The parameters required for a proper description of the phoswich are those shown in Table 1 and Fig. 3 when selecting $15 \times 2 \times 2\,mm^3$ crystals. On the other hand, the modeling of the acquisition requires the specification of time stamps resolution and dead times. Based on the presented results, the time resolution was set to 2 ns, the time window to 5 ns, and dead time was set to paralyzable/non-paralyzable 260 ns for acquisition, and non-paralyzable 800 ns for the transmission of each detected pulse.

With these settings, we have estimated the scanner's noise-equivalent count (NEC) curve for the pair of detectors in PET mode, which is shown in Fig. 5. For this purpose we placed a 2 cm radius and 5 cm height cylinder, centered inside the FOV, filled with water and with a uniform activity distribution.

Table 3
Estimated performance parameters when using two heads for each modality

	PET 2H at 511 keV	SPECT 2H at 140 keV
Sensitivity	13.1 kcps/(μCi/ml)	415 cps/(μCi/ml)
Absolute sensitivity	0.6%	0.025%
Spatial resolution (FWHM)	$<2.8\,mm^3$	$<22\,mm^3$
Max NEC	57	—
Activity at Max NEC	12.2 μCi/ml	—

For the spatial resolution estimation in PET/SPECT, five point sources equally spaced were placed along the *X*-axis. The GATE output was post-processed in order to include the required corrections In the case of PET, sinograms incorporate the DOI information which provides a uniform resolution in the complete FOV. Out of these results, we estimate some of the most relevant performance parameters of the scanner, which are shown in Table 3.

5. Conclusions

The performance of the individual detector module of a novel PET/SPECT scanner for small animals have been presented and analyzed. The YAP/LSO phoswich has been characterized in terms of optimum finish and quantum efficiency, while acquisition electronics are characterized in terms of dead time, timing resolution and layer discrimination capabilities. The extracted parameters have been used to estimate the performance of the complete system. First simulation results show the feasibility of the proposed hybrid scanner.

In the case of PET, the estimated sensitivity and NEC curves meet the expectations for two-head detectors while resolution remains almost constant for the whole FOV, thanks to the phoswich approach. However sensitivity is quite low and new architectures, with more detectors, must be analyzed if we intend to do dynamic imaging. Finally, results show that resolution degradation due to crystal misidentification is not severe as far as the error rate is kept below 10%.

Regarding SPECT, the reconstructed image shows unwanted artefacts that degrade resolution below expectations. However several issues still need to be addressed: on one hand, we believe that more sophisticated corrections may still be applied to the SPECT sinogram in order to increase resolution; on the other hand, no proper optimization has been carried out regarding the collimator. Finally, we plan to tune system parameters for SPECT imaging with low energy isotopes.

Acknowledgments

This work has been supported by FPU programme of the Spanish Education and Science Ministry, by the Spanish Thematic Network IM3 (PI052204), the joint Research Action HG04-6 and the research project TEC2004-07052-C02-02.

References

[1] R. Lecomte, Nucl. Instr. and Meth. A 527 (2004) 157.
[2] M. Kapusta, et al., IEEE Trans. Nucl. Sci. NS-47 (2000) 1341.
[3] T. Yamashita, et al., IEEE Trans. Nucl. Sci. NS-37 (1990) 594.
[4] P.D. Cutler, et al., J. Nucl. Med. 33 (1992) 595.
[5] M. Watanabe, et al., IEEE Trans. Med. Imag. 11 (1992) 577.
[6] R. Lecomte, et al., IEEE Trans. Nucl. Sci. NS-41 (1994) 1446.
[7] P.M. Bloomfield, et al., Phys. Med. Biol. 40 (1995) 1105.
[8] A.P. Jeavons, et al., IEEE Trans. Nucl. Sci. NS-46 (1999) 468.
[9] M. Streun, et al., IEEE Nucl. Sci. Symp. 2 (2001) 693.
[10] D.P. McElroy, et al., IEEE Nucl. Sci. Symp. 3 (2003) 2043.
[11] J. Seidel, et al., IEEE Trans. Nucl. Sci. NS-50 (2003) 1347.
[12] Y.-C. Tai, et al., Phys. Med. Biol. 48 (2003) 1519.
[13] C. Woody, et al., Nucl. Instr. and Meth. A 527 (2004) 166.
[14] A. Del Guerra, et al., IEEE Trans. Nucl. Sci. NS-47 (2000) 1537.
[15] E. Di-Bella, et al., J. Nucl. Med. NS-42 (2001) 944.
[16] M. Dahlbom, et al., IEEE Trans. Nucl. Sci. NS-44 (1997) 1114.
[17] A. Saoudi, R. Lecomte, IEEE Trans. Nucl. Sci. NS-46 (1999) 479.
[18] B.J. Pichler, et al., IEEE Trans. Nucl. Sci. NS-50 (2003) 1420.
[19] S. Jan, et al., Phys. Med. Biol. 49 (2004) 4543.
[20] K. Thielemans, et al., Software for Tomographic Image Reconstruction [online] 〈http://stir.hammersmithimanet.com〉
[21] F. Cayouette, et al., IEEE Trans. Nucl. Sci. NS-50 (2003) 339.
[22] P. Guerra, et al., IEEE Trans. Nucl. Sci. NS-53 (2006) 1150.
[23] M. Moszynski, et al., Nucl. Instr. and Meth. A 404 (1998) 157.
[24] P. Guerra, et al., IEEE Trans. Nucl. Sci. NS-53 (2006) 770.
[25] A.O. Hero III, IEEE Trans. Inform. Theor. 37 (1991) 92.
[26] S. Baccaro, et al., Nucl. Instr. and Meth. A 406 (1998) 479.
[27] C.W.E. van Eijk, Nucl. Instr. and Meth. A 460 (2001).
[28] H. Rothfuss, et al., IEEE Trans. Nucl. Sci. NS-51 (2004) 770.
[29] Hamamatsu, H8500 Datasheet, 2003.
[30] C. Moisan, et al., IEEE Trans. Nucl. Sci. NS-44 (1997) 1219.